Supporting Information

Integrating Solid Interfaces for Catalysis in All-Solid-State Lithium-Sulfur Batteries

Yun Cao,[†a] Chuannan Geng,[†ab] Chen Bai,[a] Linkai Peng,[a] Jiaqi Lan,[a] Jiarong Liu,[c] Junwei Han,[d] Bilu Liu,[c] Yanbing He,[a] Feiyu Kang,[a] Quan-Hong Yang[b] and Wei Lv,*[a]

[a]Shenzhen Geim Graphene Center, Engineering Laboratory for Functionalized Carbon Materials, Tsinghua Shenzhen International Graduate School, Tsinghua University, Shenzhen, 518055, China.

[b]Nanoyang Group, Tianjin Key Laboratory of Advanced Carbon and Electrochemical Energy Storage, School of Chemical Engineering and Technology, National Industry-Education Intergration Platform of Energy Storage Collaborative Innovation Center of Chemical Science and Engineering (Tianjin), Tianjin University, Tianjin, 300072, China.

[c]Shenzhen Key Laboratory of Advanced Layered Materials for Value-added Applications, Tsinghua-Berkeley Shenzhen Institute and Institute of Materials Research, Tsinghua Shenzhen International Graduate School, Tsinghua University, Shenzhen 518055, China.

[d]Research Center on Advanced Chemical Engineering and Energy Materials, China University of Petroleum (East China), Qingdao 266580, China.

* E-mail: lv.wei@sz.tsinghua.edu.cn

† These authors contributed equally to this work.

Keywords: All-solid-state Li-S batteries; Molecular-level Interfaces; Catalysis; Micropores.

Supporting Figures

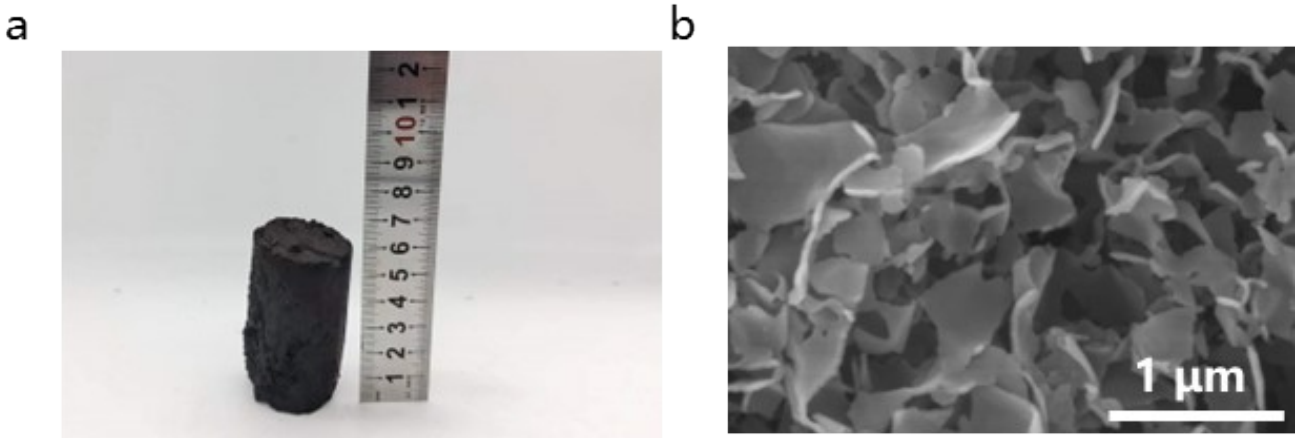

Fig. S1 (a) The monolith formed after hydrothermal treatment of glucose with GO and the corresponding (b) SEM image.

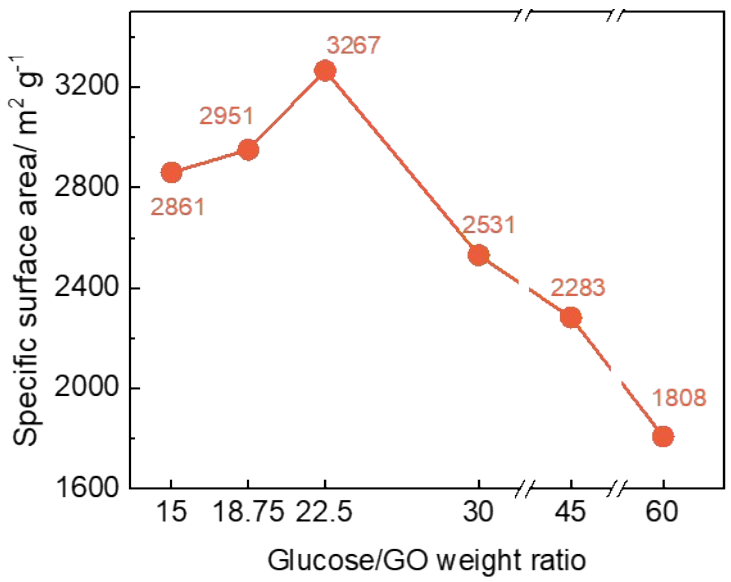

Fig. S2 Glucose/GO weight ratio adjustment of MCS carbon.

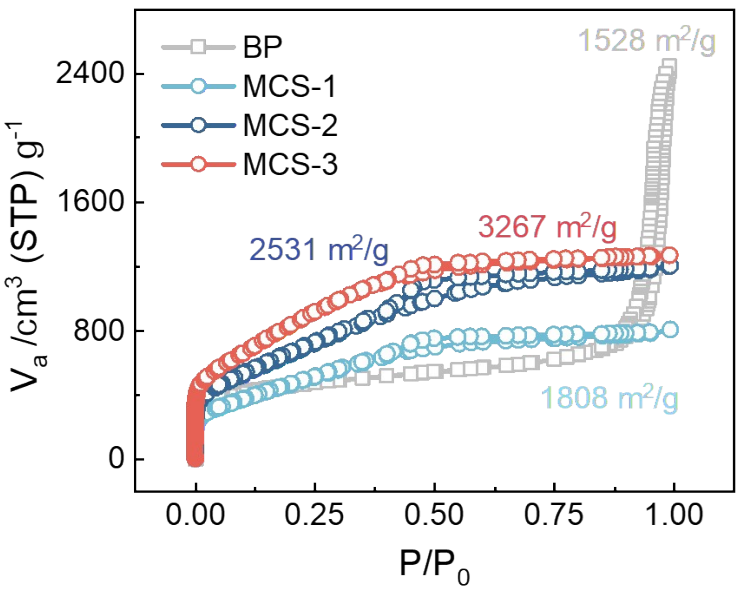

Fig. S3 Nitrogen adsorption-desorption isotherms of BP, MCS-1, MCS-2 and MCS-3 and the specific surface areas calculated by Brunauer-Emmett-Teller method.

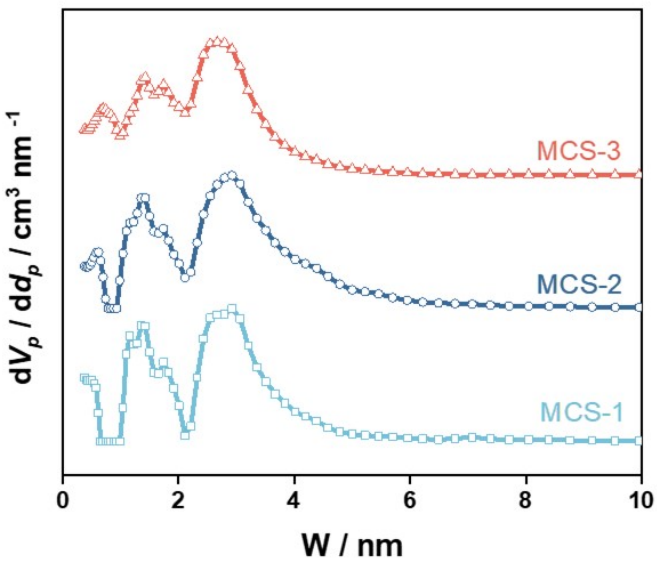

Fig. S4 Pore size analysis of BP, MCS-1, MCS-2 and MCS-3 by non-local density functional theory method.

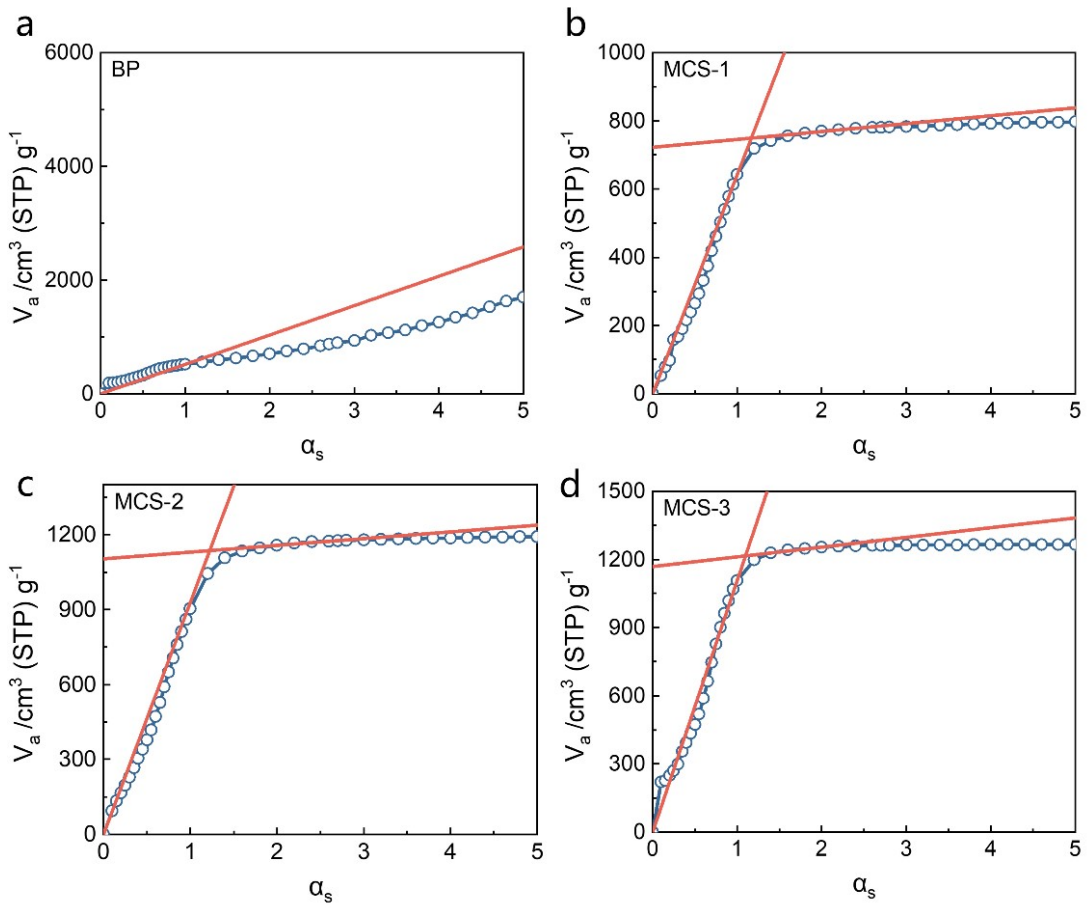

Fig. S5 α_s plots of (a) BP, (b) MCS-1, (c) MCS-2 and (d) MCS-3.

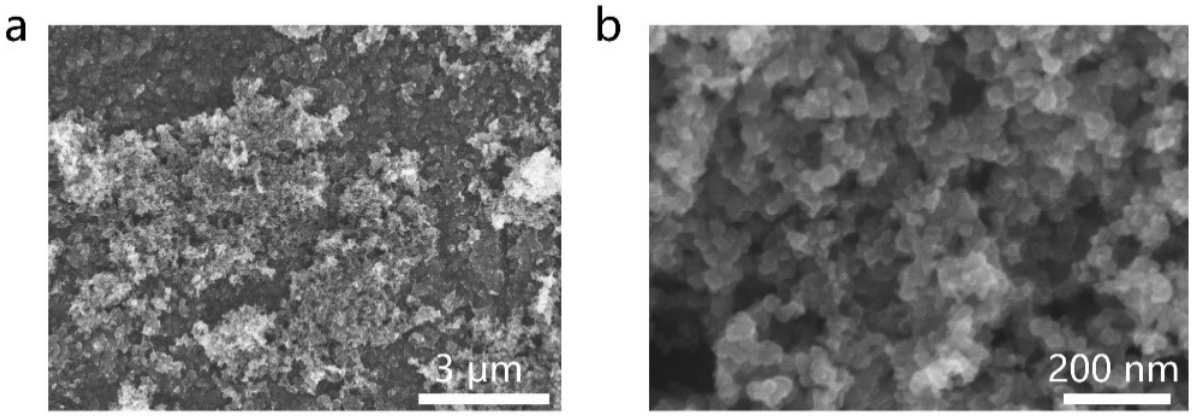

Fig. S6 SEM images of BP.

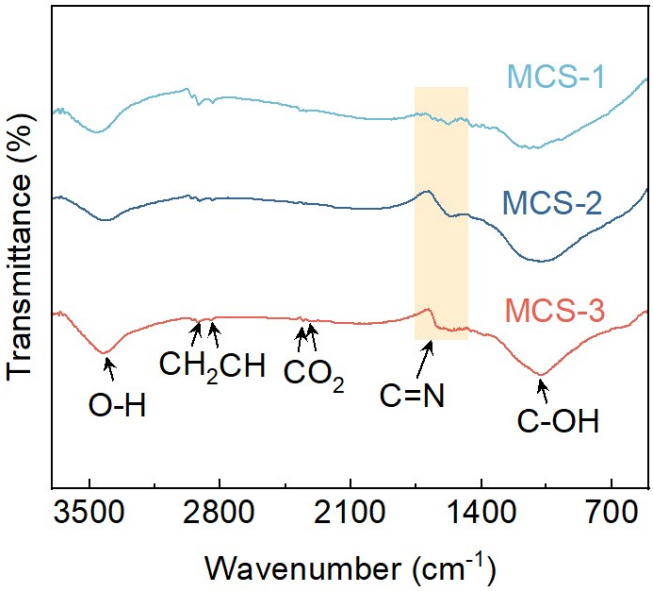

Fig. S7 Fourier transform infrared spectrometer spectra of MCS-1, MCS-2 and MCS-3.

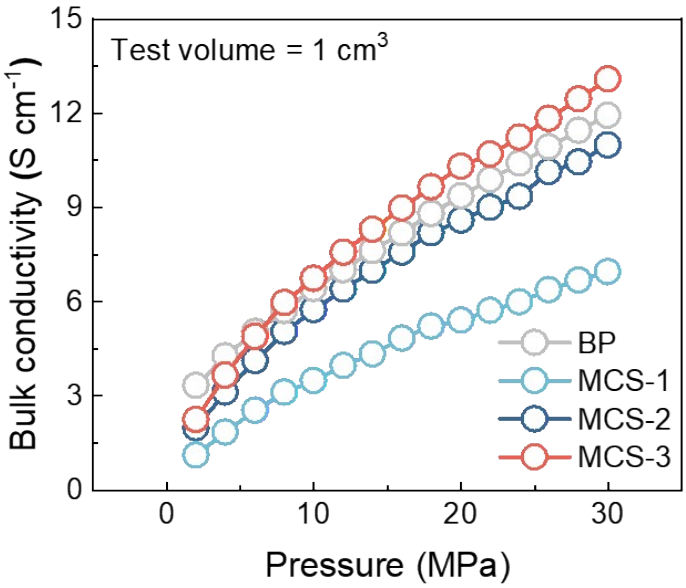

Fig. S8 Bulk conductivities of BP, MCS-1, MCS-2 and MCS-3.

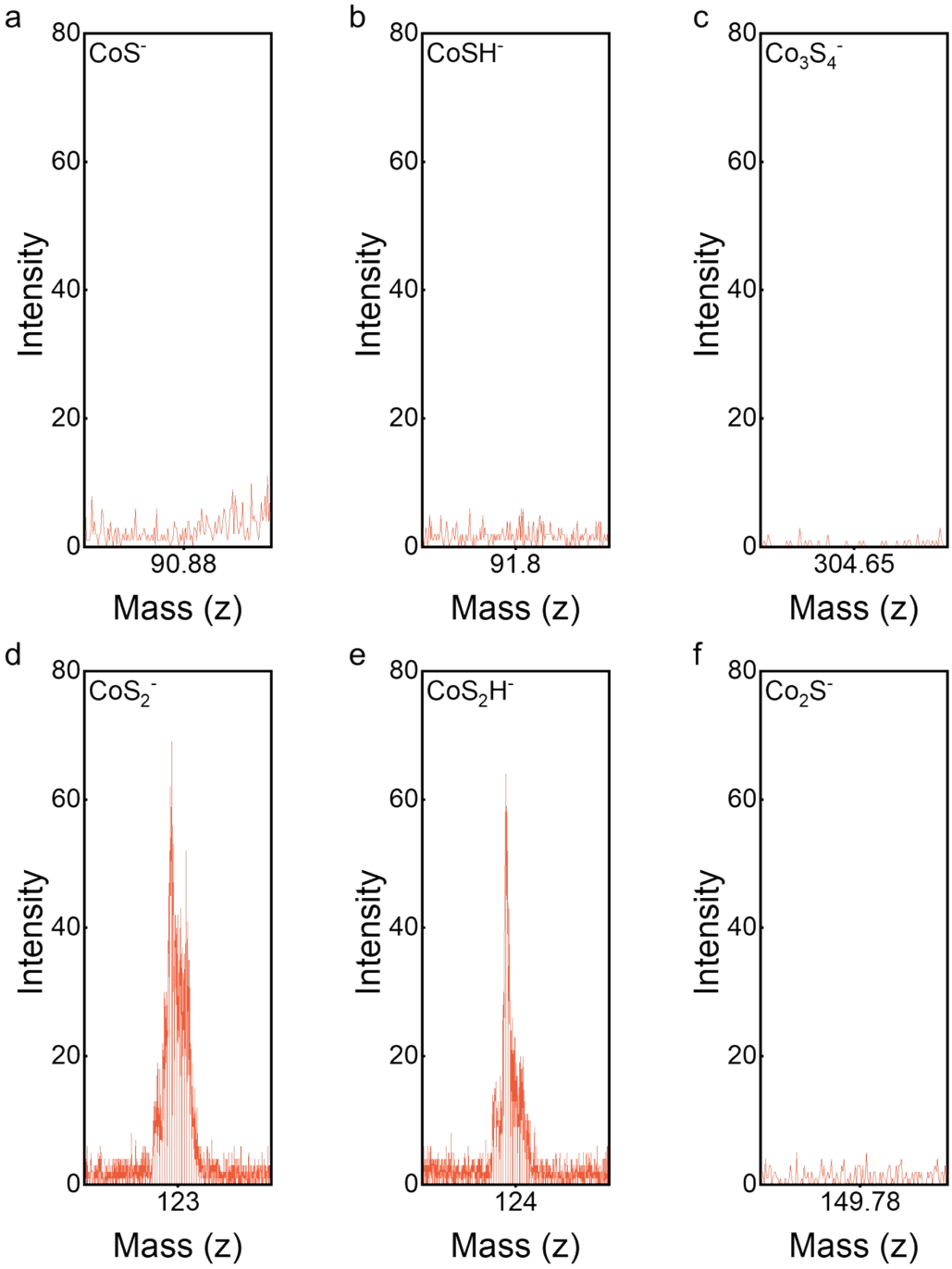

Fig. S9 TOF-SIMs spectrum of a) CoS^-; b) $CoSH^-$; c) $Co_3S_4^-$; d) CoS_2^-; e) CoS_2H^-; f) $Co2S^-$.

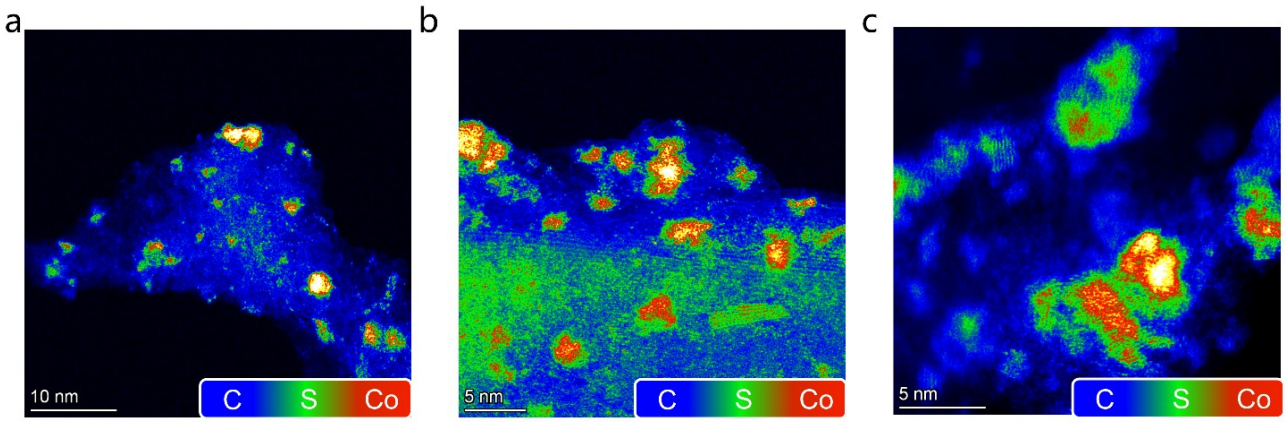

Fig. S10 HAADF-STEM images of MCS-3-S-Co (colored according to the scattering intensity).

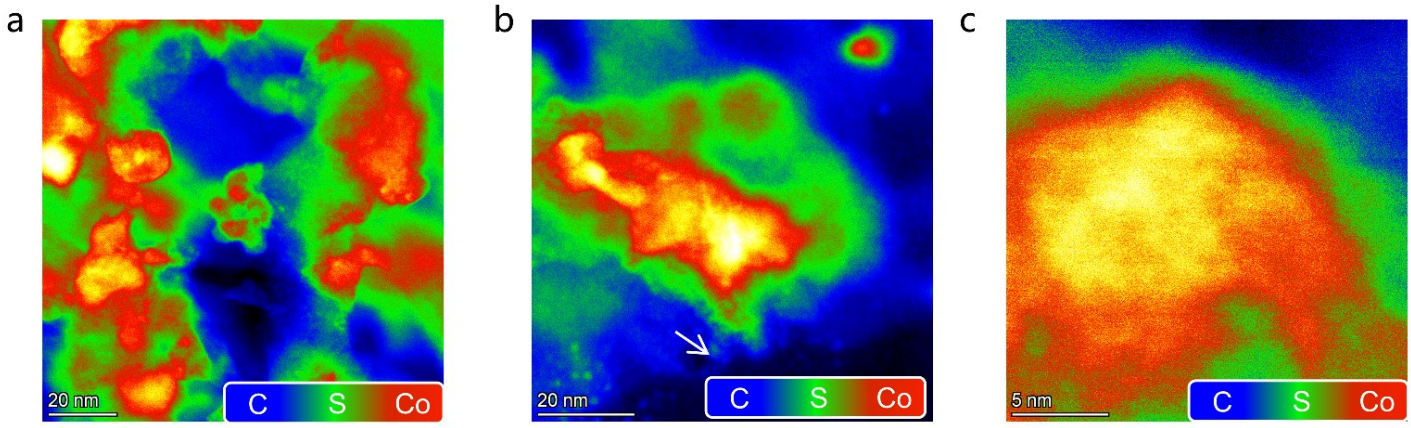

Fig. S11 HAADF-STEM images of BP-S-Co particles (colored according to the scattering intensity).

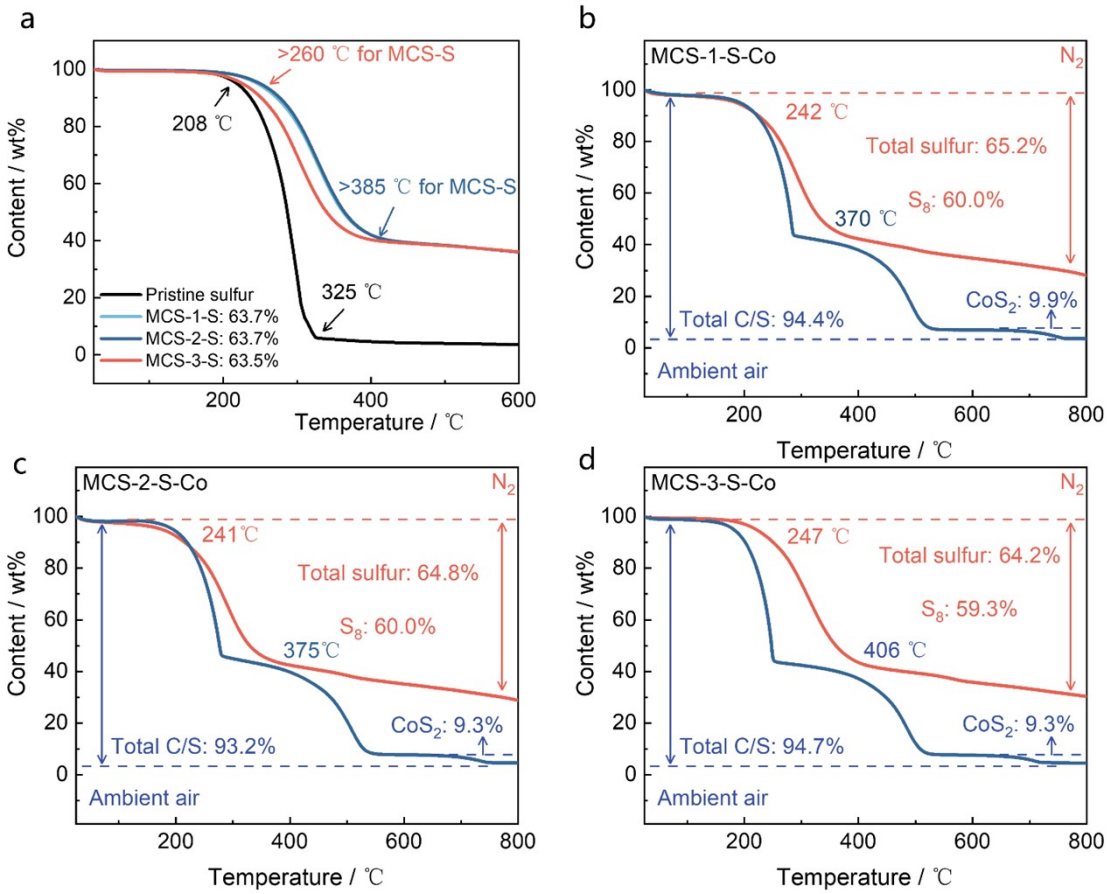

Fig. S12 (a) TGA curves of MCS-1-S, MCS-2-S and MCS-3-S under N_2 atmosphere. (b-d) TGA curves of MCS-1-S-Co, MCS-2-Co and MCS-3-Co under N_2 and air atmosphere.

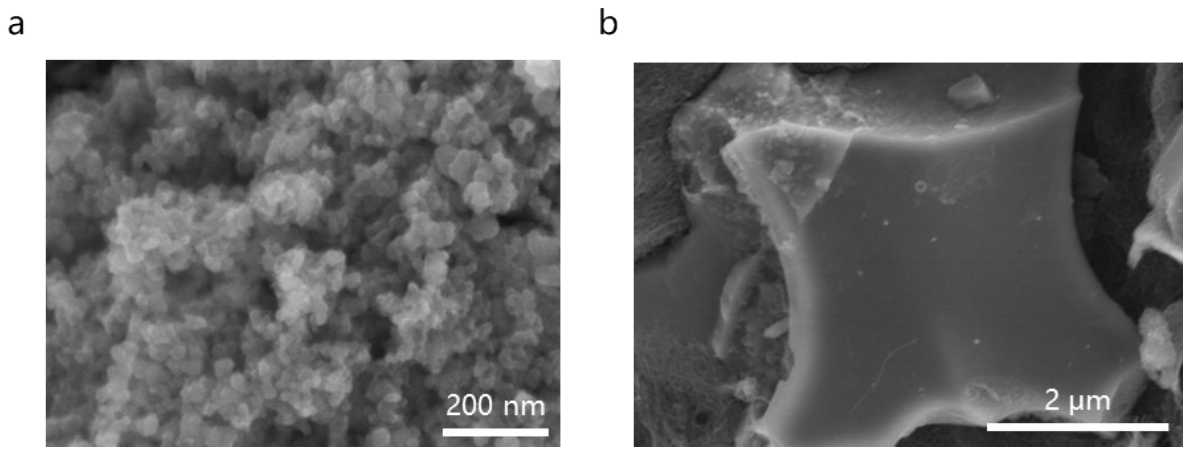

Fig. S13 SEM images of (a) BP-S-Co and (b) MCS-3-S-Co.

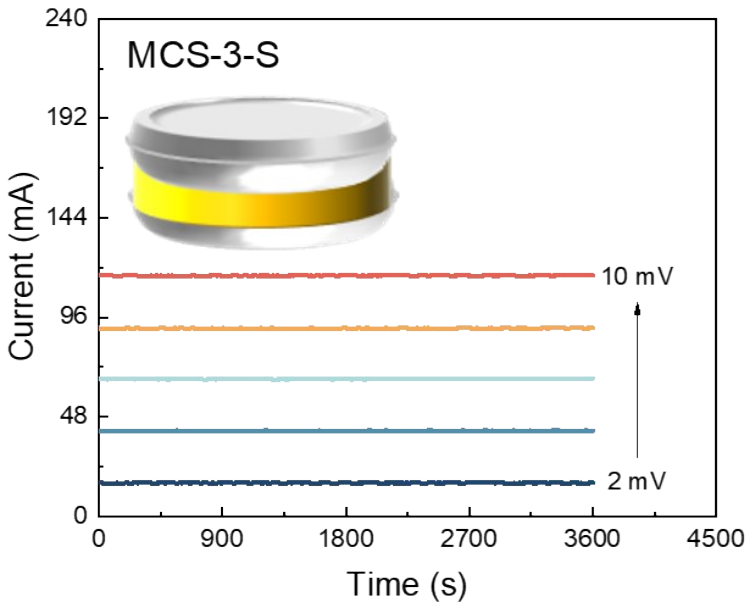

Fig. S14 DC polarization measurement of MCS-3-S.

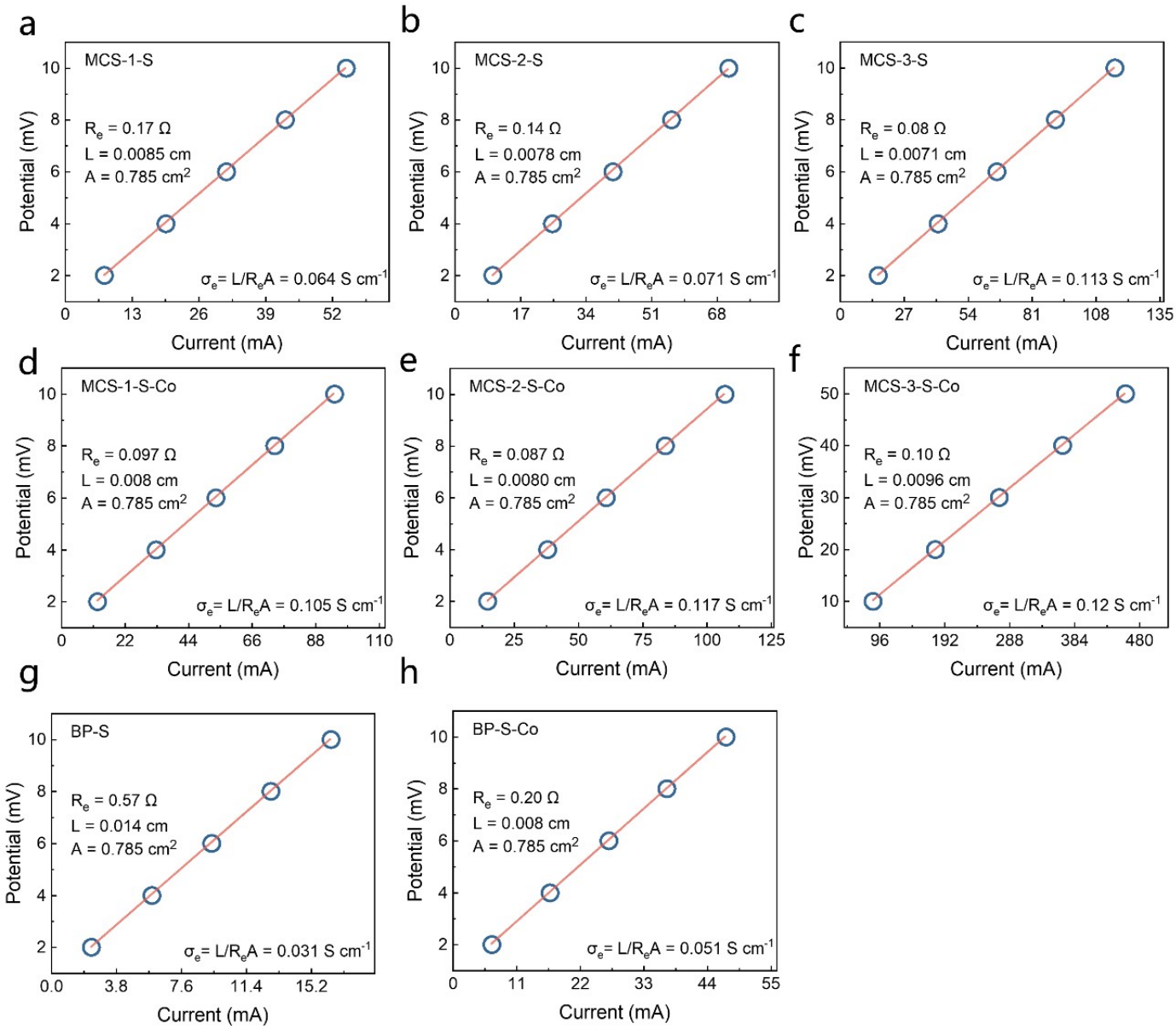

Fig. S15 Linear fittings of DC polarization results for different cathodes: (a) MCS-1-S, (b) MCS-2-S, (c) MCS-3-S, (d) MCS-1-S-Co, (e) MCS-2-S-Co, (f) MCS-3-S-Co, (g) BP-S and (h) BP-S-Co.

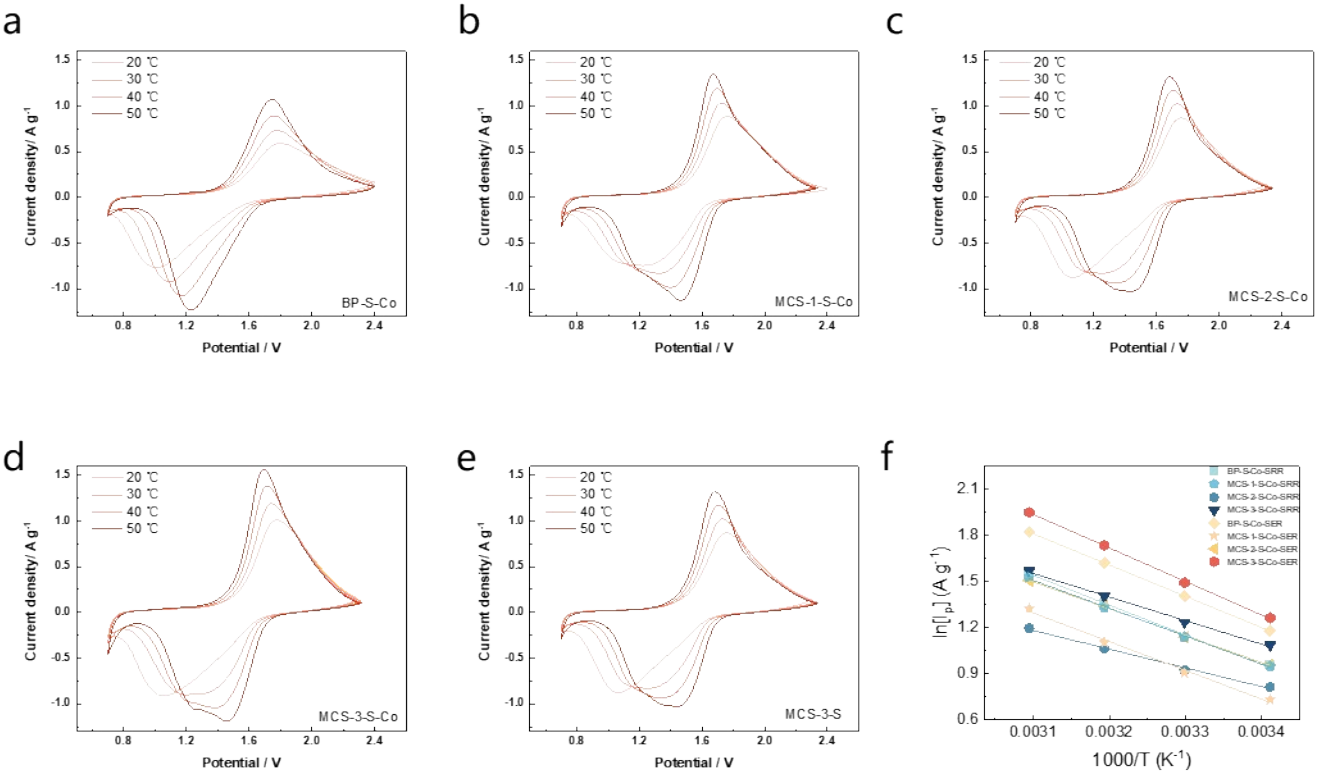

Fig. S16 CV curves at different temperatures for (a) BP-S-Co, (b) MCS-1-S-Co, (c) MCS-2-S-Co, (d) MCS-3-S-Co and (d) MCS-3-S. (f) Corresponding Arrhenius plots calculated by peak currents.

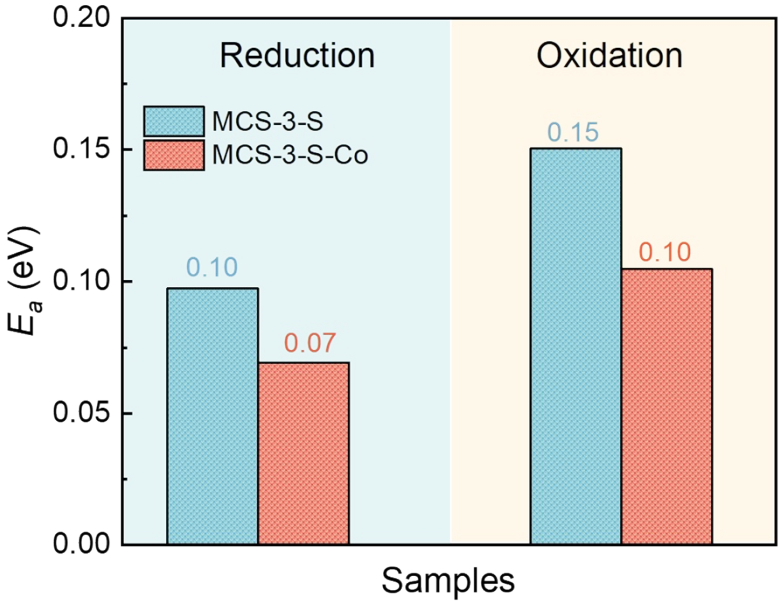

Fig. S17 Comparisons MCS-3-S and MCS-3-S-Co electrodes.

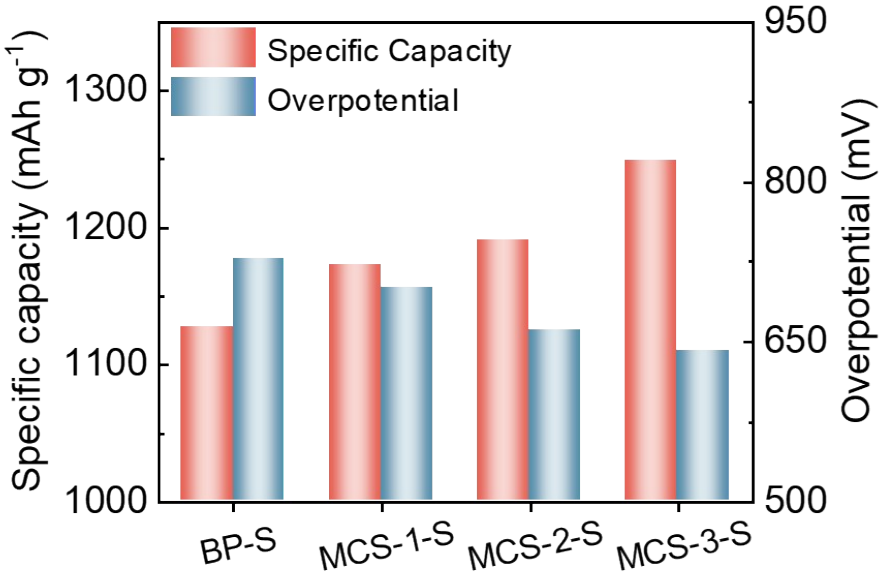

Fig. S18 Specific capacity and overpotential analysis of BP-S, MCS-1-S, MCS-2-S and MCS-3-S cathodes.

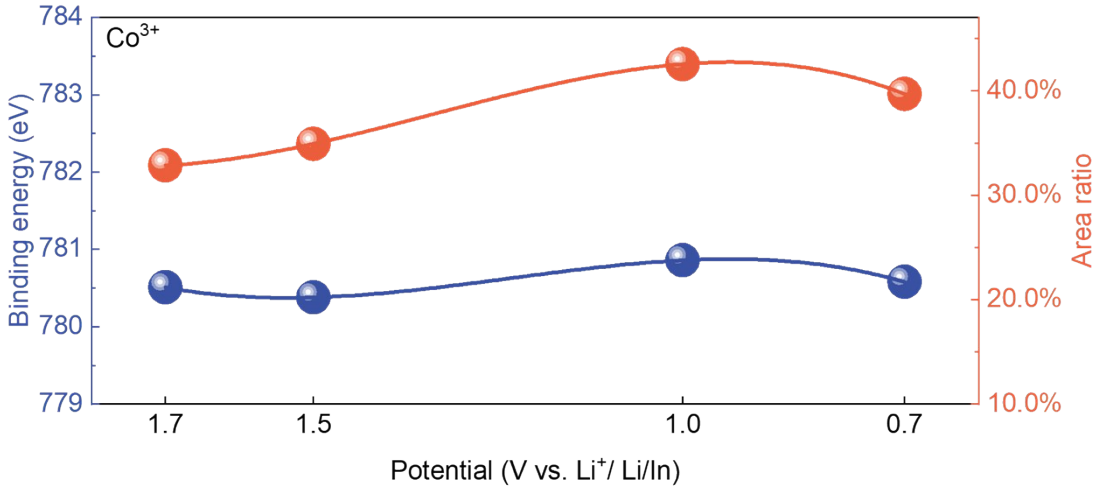

Fig. S19 Binding energy and peak area ratio analysis of Co^{3+} during discharge.

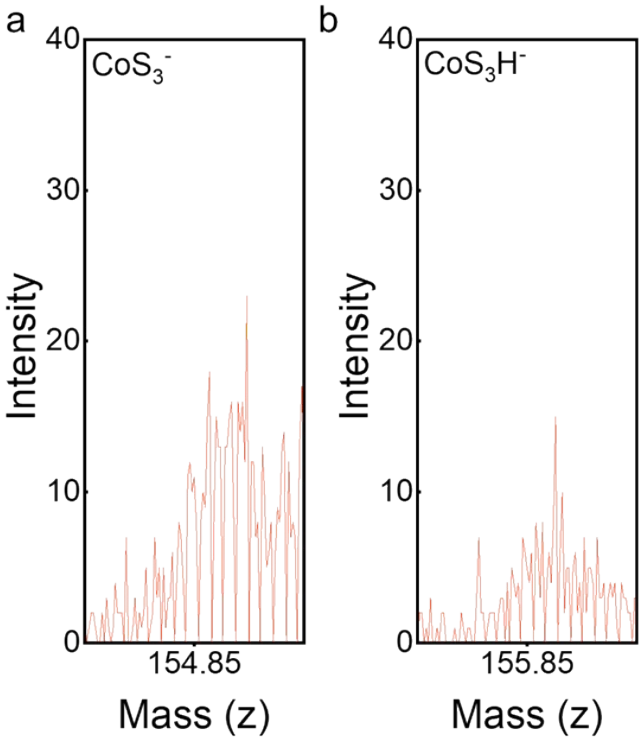

Fig. S20 TOF-SIMs spectrum of a) CoS_3^-; b) CoS_3H^-.

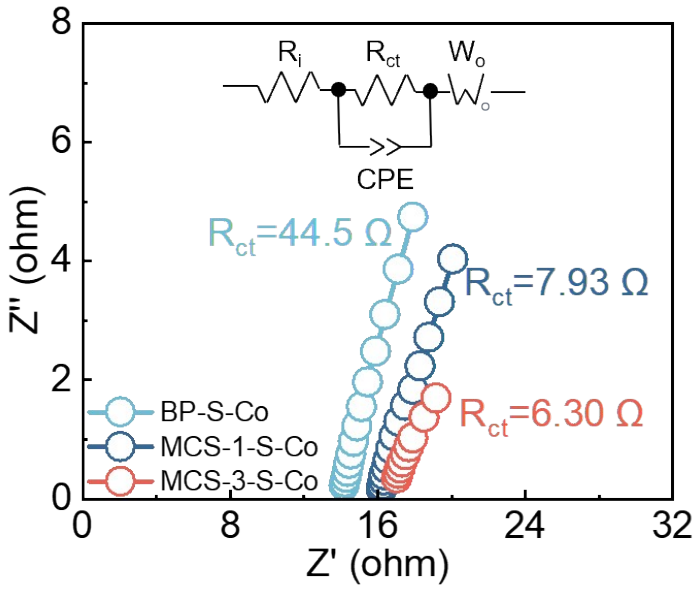

Fig. S21 EIS measurement results of BP-S-Co, MCS-1-S-Co, and MCS-3-S-Co cathodes.

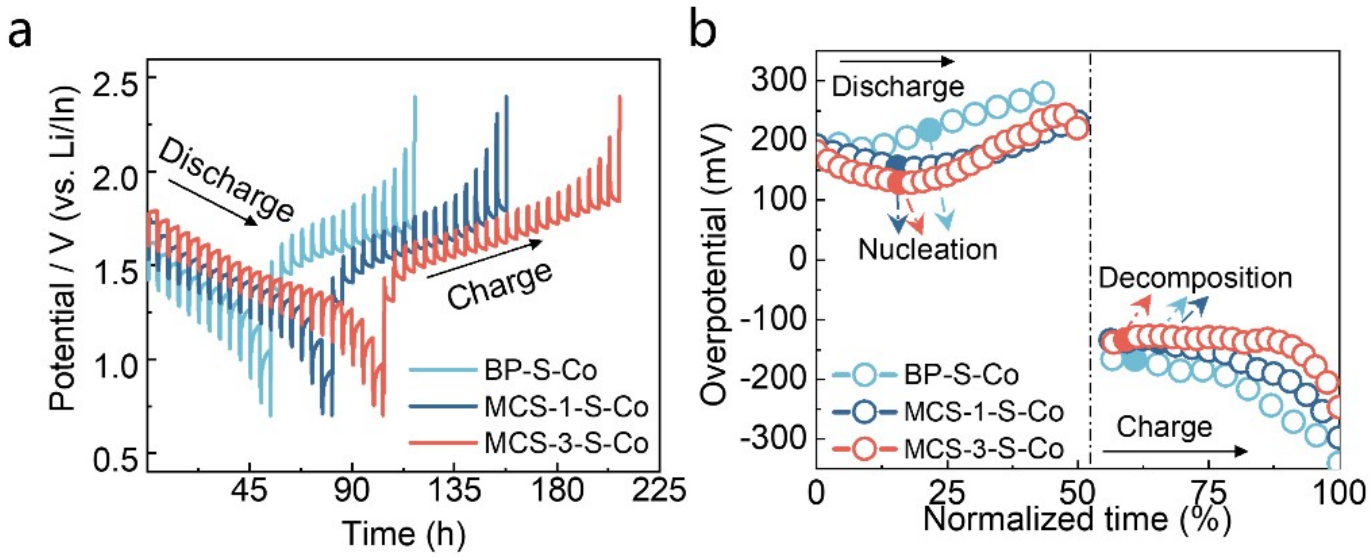

Fig. S22 (a) GITT measurement results and (b) corresponding overpotentials for BP-S-Co, MCS-1-S-Co, and MCS-3-S-Co cathodes.

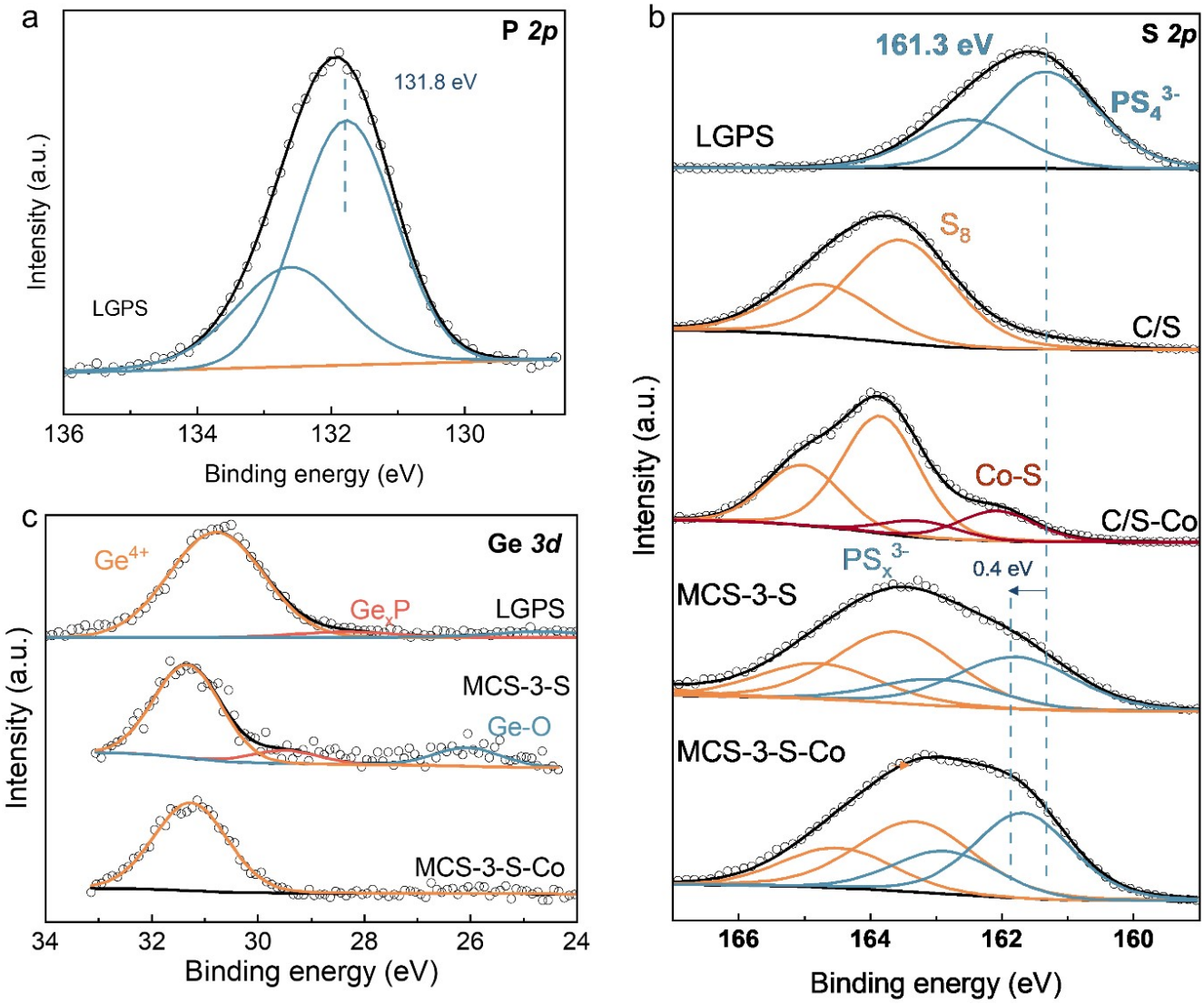

Fig. S23 (a) P *2p*, (b) S *2p* and (c) Ge *3d* XPS results of LGPS, MCS-S-3 and MCS-S-3-Co.

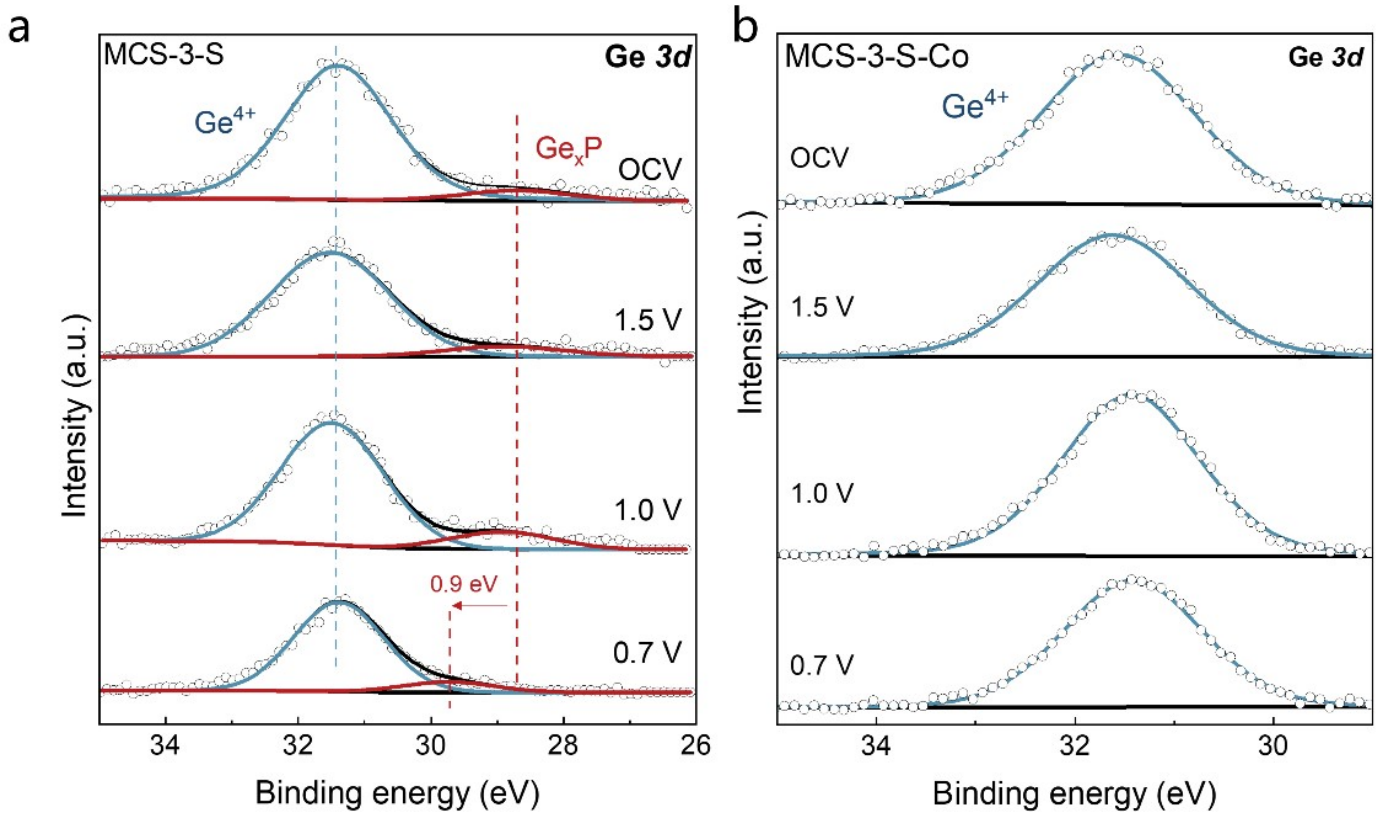

Fig. S24 Ge *3d* XPS results of (a) MCS-3-S and (b) MCS-3-S-Co cathodes at different potentials.

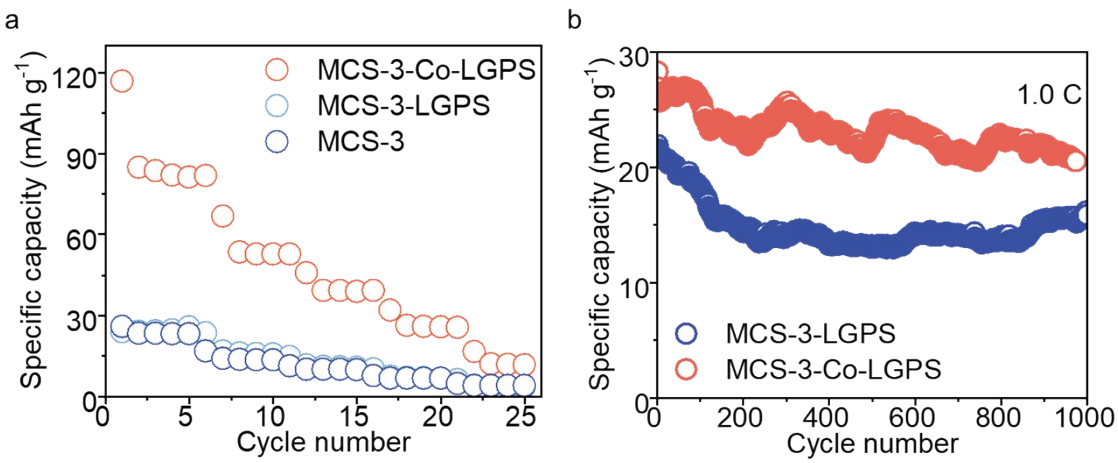

Fig. S25 a) Rate performance of MCS-3, MCS-3-LGPS and MCS-3-Co-LGPS cathode; b) Cycling performance of MCS-3-LGPS and MCS-3-Co-LGPS cathode cathode at 1.0 C. (MCS-3 refers to the pristine carbon cathode; MCS-3-LGPS refers to the cathode of ball-milled MCS-3 and LGPS; MCS-3-Co-LGPS refers to the cathode of ball-milled MCS-3, LGPS, CoS_2)

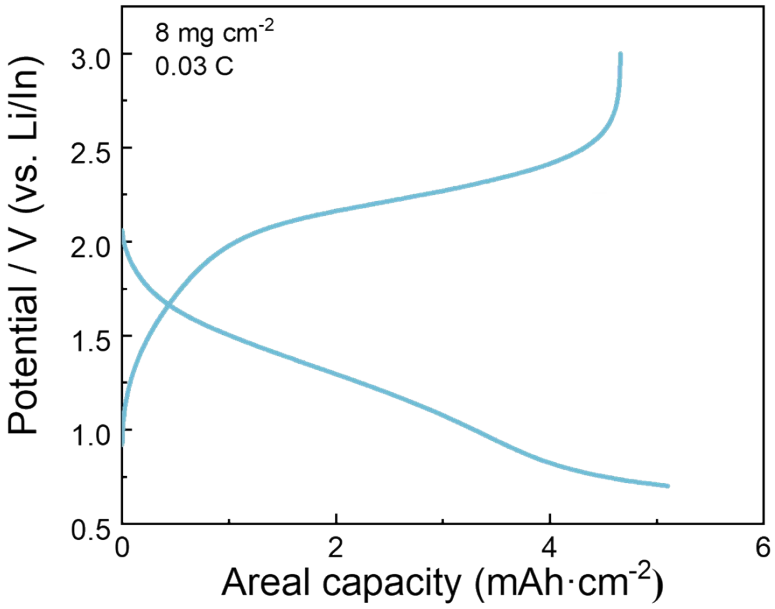

Fig. S26 Galvanostatic charge-discharge profile of MCS-3-S-Co at 0.03 C with a sulfur loading of 8 mg cm^{-2}.

Supporting Tables

Table S1. Specific surface area distribution with different preparation parameters.

Glucose/GO weight ratio	**KOH concentration/ g mL^{-1}**	**Activation temperature / ℃**	**Specific surface area / m^2 g^{-1}**
15	1	800	2861
18.75	1	800	2951
22.5	1	800	3267
30	1	800	2531
45	1	800	2283
60	1	800	1808
22.5	1	900	2511
22.5	1.5	800	2877
22.5	2	800	2493

Table S2. SSA and micropore volume of different microporous carbons.

Sample name	SSA / m^2 g^{-1}	Micropore volume / cm^3 g^{-1}	Reference
ACC-10	1094	0.4	[1]
ACC-15	1436	0.5	
APC-1050	1496	0.8	
BP	1528	0	This Work
APC-950	1555	0.8	Ref[1]
APC-1000	1569	0.8	
AEL-1200	1602	0.7	
AEL-1100	1685	0.7	
YP-50F	1694	0.7	
APC-700-2	1700	0.8	
AEL-1000	1701	0.8	
APC-700-1	1708	0.8	
EL-104	1721	0.8	
PW-400	1724	0.8	
APC-1100	1761	0.9	
ACS-PC	1796	0.9	
MC	1800	0.5	Ref[2]
***MCS-1**	**1808**	**1.2**	This Work
APC-800	1815	0.9	Ref[1]
SC-1800	1821	0.8	
EL-106	1907	0.9	
ACC-20	2004	0.8	
YP-80F	2264	1.1	
***MCS-2**	**2528**	**1.8**	This Work
aMP	3160	1.6	Ref[3]
***MCS-3**	**3267**	**2.0**	This Work
BL-1/4	3557	1.4	Ref[4]

References

1 X. Liu, D. Lyu, C. Merlet, M. J. A. Leesmith, X. Hua, Z. Xu, C. P. Grey and A. C. Forse, *Science (80-.).*, 2024, **384**, 321–325.

2 S. Zheng, F. Yi, Z. Li, Y. Zhu, Y. Xu, C. Luo, J. Yang and C. Wang, *Adv. Funct. Mater.*, 2014, **24**, 4156–4163.

3 C. W. Huang, C. Te Hsieh, P. L. Kuo and H. Teng, *J. Mater. Chem.*, 2012, **22**, 7314–7322.

4 L. Estevez, V. Prabhakaran, A. L. Garcia, Y. Shin, J. Tao, A. M. Schwarz, J. Darsell, P. Bhattacharya, V. Shutthanandan and J. G. Zhang, *ACS Nano*, 2017, **11**, 11047–11055.